

# Game-theoretic modeling of collective decision-making during epidemics

Mengbin Ye<sup>1</sup>, Lorenzo Zino<sup>2</sup>, Alessandro Rizzo<sup>3,4</sup>, Ming Cao<sup>2</sup>

<sup>1</sup>Optus–Curtin Centre of Excellence in Artificial Intelligence, Curtin University, Perth, Australia

<sup>2</sup>Faculty of Science and Engineering, University of Groningen, 9747 AG Groningen, Netherlands

<sup>3</sup>Department of Electronics and Telecommunications, Politecnico di Torino, 10129 Turin, Italy

<sup>4</sup>Office of Innovation, New York University Tandon School of Engineering, Brooklyn NY 11201, USA

Correspondence should be addressed to: [mengbin.ye@curtin.edu.au](mailto:mengbin.ye@curtin.edu.au)

arXiv:2008.01971v3 [q-bio.PE] 13 May 2021

## Abstract

We introduce a parsimonious game-theoretic behavioral–epidemic model, in which an interplay of realistic factors shapes the co-evolution of individual decision-making and epidemics on a network. Although such a co-evolution is deeply intertwined in the real-world, existing models schematize population behavior as instantaneously reactive, thus being unable to capture human behavior in the long term. Our model offers a unified framework to model and predict complex emergent phenomena, including successful collective responses, periodic oscillations, and resurgent epidemic outbreaks, as illustrated through two real-world case studies.

The collective adoption of appropriate behavior by a population is crucial to respond to an epidemic, especially when pharmaceutical interventions are absent or logistical challenges prevent their widespread deployment [1]. However, classical mathematical epidemic models often consider oversimplified behavioral response [2]. To fill in this gap, awareness-based models have been proposed [3–9], in which the epidemic process co-evolves with the spread of the awareness of the outbreak. While these models have demonstrated effectiveness in capturing the early-stage, immediate behavioral response to an epidemic, they are limited because they assume fully rational, purely instantaneous, and reactive decision-making in the population. Such models therefore fail to capture the very range of factors that affect real-world behavioral responses over the whole course of an epidemic, such as social influence [10], perceived infection risk [11], accumulating fatigue and socio-economic costs [12, 13], bounded rationality in individuals’ decisions [14], and the impact of government-mandated interventions [15].

The world is not new to epidemics that evolve over long time horizons of several months or even years, persisting until effective drugs and vaccines are developed and made widely available [16], making purely reactive models of limited efficacy. This calls for a paradigm shift in mathematical modeling, from reactive and fully rational behavioral responses [3–6, 8, 9], to a long-term outlook where complex behavioral dynamics arise at the individual-level and co-evolve at the same time scale of the epidemic spreading. Game-theoretic models have proved to be effective to reproduce similar complex decision-making mechanisms, thereby capturing realistic behavioral responses in several fields [17].

Here, we propose a game-theoretic model that accounts for long-term and bounded-rational decision-making, which is able to reproduce the complex and concurrent evolution of behavioral response and epidemic spreading, that is well-known and documented in the real-world [1]. Several efforts have been proposed across similar research avenues, although with different and narrower angles. For example, imitation mechanisms [11, 13, 18, 19] rely on a population-level modeling that can capture only limited features of such complex behavioral dynamics, and game-theoretic modeling of vaccination adoption [20–25] relies on a time-scale separation between the decision-making and the epidemics, which does not capture general behavioral response. Here, we adopt a network approach with individual granularity [2] and a co-evolution of the two processes, at the same time scale. Hence, our model is able to capture the individual-level responses and time-varying contagion patterns, whose *co-evolution* collectively shapes the epidemic outbreak. Our approach enables the *explicit and concurrent* inclusion of the most salient factors that each individual trades off when deciding their time-varying behavioral response to an ongoing epidemic. We propose a unified and parsimonious mathematical framework, which is able to capture and reproduce complex realistic behavioral response by the population, including successful collective responses leading to the eradication of the disease, periodic oscillations, and weak responses leading to the emergence of multiple epidemic waves.

We consider a population  $\mathcal{V}$  of  $n$  individuals. Each individual  $i \in \mathcal{V}$  is characterized by a two-dimensional variable  $(x_i(t), y_i(t))$ , which models their *social behavior* and *health state* at the discrete time  $t \in \mathbb{Z}_{\geq 0}$ , respectively. The social behavior of individual  $i$  is captured by the binary variable  $x_i(t) \in \{0, 1\}$ , which expresses whether  $i$  adopts self-protective behaviors ( $x_i(t) = 1$ ), such as physical distancing [1], or discards this opportunity ( $x_i(t) = 0$ ). The health state  $y_i(t)$  takes values

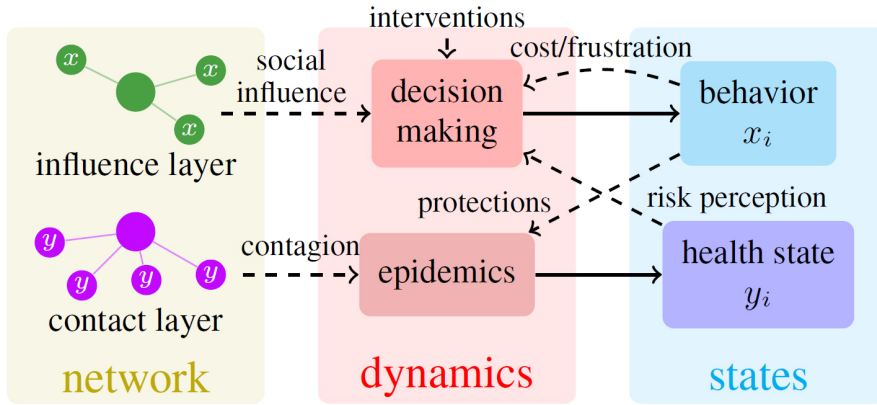


Figure 1: Schematic of the co-evolutionary paradigm.

in a discrete set of compartments  $\mathcal{A}$ . For example,  $\mathcal{A} = \{S, I\}$  is selected to model the susceptible–infected–susceptible (SIS) epidemic process exemplified in this work [26]. A global observable  $z(t)$  quantifies the *detectable prevalence* of the epidemic at time  $t$ :  $z(t) := \frac{1}{n} |\{i : y_i(t) = I\}|$ , where  $|\cdot|$  denotes a set’s cardinality. The paradigm is amenable to extensions to capture different levels of protection through the selection of a different support for  $x_i(t)$ , while further compartments added to  $\mathcal{A}$  can capture additional features of the epidemic process [26].

The decision-making and disease spreading in the population co-evolve, mutually influencing each other on a two-layered [27] network  $\mathcal{G} = (\mathcal{V}, \mathcal{E}_I, \mathcal{E}_C(t))$ , as schematized in Fig. 1. The set of undirected links  $\mathcal{E}_I$  defines the static *influence layer*, capturing *social influence* between individuals in their decision-making processes. The *contact layer* is defined through a time-varying set of undirected links  $\mathcal{E}_C(t)$ , which represent the *physical contacts* between pairs of individuals that are the avenues for the transmission of the disease. The temporal formation mechanism of the contact layer is general, and can be generated according to any model of time-varying networks [28–33].

At each discrete time-step  $t$ , every individual  $i$  enacts a decision-making process on the adoption of self-protective behaviors, according to an evolutionary game-based mechanism termed logit learning [34]. We define two *payoff* functions  $\pi_i^0(t)$  and  $\pi_i^1(t)$ , which represent a combination of socio-psychological, economic, and personal benefits received by individual  $i$  for enacting behaviors  $x_i = 0$  and  $x_i = 1$  at time  $t$ , respectively. This individual then adopts self-protective behaviors with a probability equal to

$$\mathbb{P}[x_i(t+1) = 1] = \frac{\exp\{\beta\pi_i^1(t)\}}{\exp\{\beta\pi_i^0(t)\} + \exp\{\beta\pi_i^1(t)\}}; \quad (1)$$

otherwise the individual will adopt  $x_i(t+1) = 0$ . The parameter  $\beta \in [0, \infty)$  measures an individual’s *rationality* in the decision-making process; the larger is  $\beta$ , the higher the probability that the individual chooses the behavior that maximizes their payoff. Payoffs are defined as

$$\pi_i^0(t) := \frac{1}{d_i} \sum_{j:(i,j) \in \mathcal{E}_I} (1 - x_j(t)) - u(t), \quad (2a)$$

$$\pi_i^1(t) := \frac{1}{d_i} \sum_{j:(i,j) \in \mathcal{E}_I} x_j(t) + r(z(t)) - f_i(t), \quad (2b)$$

where  $d_i := |\{j : (i, j) \in \mathcal{E}_I\}|$  is the degree of node  $i$  on the influence layer, and contain the following four terms.

**Social influence.** The first term in Eqs. (2a)–(2b), inspired by network coordination games [35], captures the *social influence* of neighboring individuals and the individual’s desire to coordinate with them on the behavioral response [10]. An increased payoff is provided for conforming to the behavior adopted by the majority of individual  $i$ ’s neighbors.

Table 1: Notation.

$n$	population size	$\lambda$	infection probability
$\mathcal{E}_I$	influence layer edges	$\mu$	recovery probability
$\mathcal{E}_C(t)$	contact layer edges	$\beta$	rationality
$N_i(t)$	infectious contacts of $i$	$u(t)$	policy interventions
$d_i$	influence degree of $i$	$r(z)$	risk perception function
$x_i(t)$	behavior of $i$	$c$	immediate cost
$y_i(t)$	health state of $i$	$\gamma$	accumulation factor
$z(t)$	detected prevalence	$f_i(t)$	frustration function of $i$

**Policy interventions.** The time-varying term  $u(t) \geq 0$  in Eq. (2a) captures *nonpharmaceutical interventions* enforced by public authorities to discourage dangerous behaviors, e.g., lockdowns, see [15] for more details.

**Risk perception.** The *risk-perception function*  $r(z) : [0, 1] \rightarrow \mathbb{R}_{\geq 0}$  in Eq. (2b) is a monotonically nondecreasing function of the detectable prevalence  $z$ , which models an incentive to adopt self-protective behavior due to the endogenous fear of becoming infected as the disease spreads, or to abandon them due to the growing optimism of returning to normal as the epidemic dwindles. This function is amenable to several generalizations, e.g., to capture imperfect or delayed information, or heterogeneity in the population.

**Cost of self-protective behavior.** The negative impact of adopting self-protections is captured in Eq. (2b) by the *frustration function*  $f_i(t) = c + \sum_{s=1}^t \gamma^s c x_i(t-s)$ , where  $c \geq 0$  quantifies the social, psychological, and economic *immediate cost* per unit-time, and  $\gamma \in [0, 1]$  is its *accumulation factor* [13, 36]. When  $\gamma = 0$ , individuals accounts only for the immediate cost while, the larger the  $\gamma$ , the higher the impact of past decisions on the payoff.

Concurrently with the behavioral decision, at each time-step  $t$ , every individual  $i$  that does not adopt self-protections and is susceptible (i.e.,  $x_i(t) = 0$  and  $y_i(t) = S$ ) may become infected upon contact with an infected individual  $j : y_j(t) = I$ , with a per-contact *infection probability*  $\lambda \in [0, 1]$ . We assume that the adoption of self-protection,  $x_i(t) = 1$ , is always successful in preventing contagion, but does not affect the individual’s probability of transmitting the disease (the model can be extended to account for imperfect and mutual protection). Hence, considering an SIS epidemic model, the contagion probability for individual  $i \in \mathcal{V}$  evolves in time as

$$\mathbb{P}[y_i(t+1) = I | y_i(t) = S] = (1 - x_i(t)) \left( 1 - (1 - \lambda)^{N_i(t)} \right), \quad (3)$$

where  $N_i(t) = |\{j \in \mathcal{V} : (i, j) \in \mathcal{E}_C(t), y_j(t) = I\}|$  is the number of infectious physical contacts of node  $i$  at time  $t$ . Besides the contagion, at each time-step  $t$ , every infected individual  $i$  recovers with probability  $\mu \in (0, 1]$ , becoming susceptible again to the disease, i.e.,  $\mathbb{P}[y_i(t+1) = S | y_i(t) = I] = \mu$ . Table 1 summarizes the notation.

In the following, we opt for modeling the contact layer  $\mathcal{E}_C(t)$  by means of a discrete-time activity-driven network (ADN) [29], due to its simplicity and ability to capture the temporal and heterogeneous nature of real-world networks. In ADNs, each individual  $i \in \mathcal{V}$  is characterized by a constant parameter  $a_i \in [0, 1]$ , called *activity*, which quantifies their probability to be “active” and thus generate a fixed number  $m \geq 1$  of undirected links with other individuals selected uniformly at random from the population, for each discrete-time step  $t$ .

For large populations and fully connected influence layers, we compute the epidemic threshold via a mean-field approach [37]. In the absence of cumulative frustration ( $\gamma = 0$ ), which is a reasonable assumption in the early stages of an outbreak, and assuming constant policy interventions  $u(t) = \bar{u}$ , the outbreak is quickly eradicated if

$$\frac{\lambda}{\mu} < \frac{e^{\beta(1-\bar{u})} + (1-\beta)e^{-\beta c}}{m(\langle a \rangle + \sqrt{\langle a^2 \rangle})(e^{\beta(1-\bar{u})} - \beta e^{-\beta c})}, \quad (4)$$

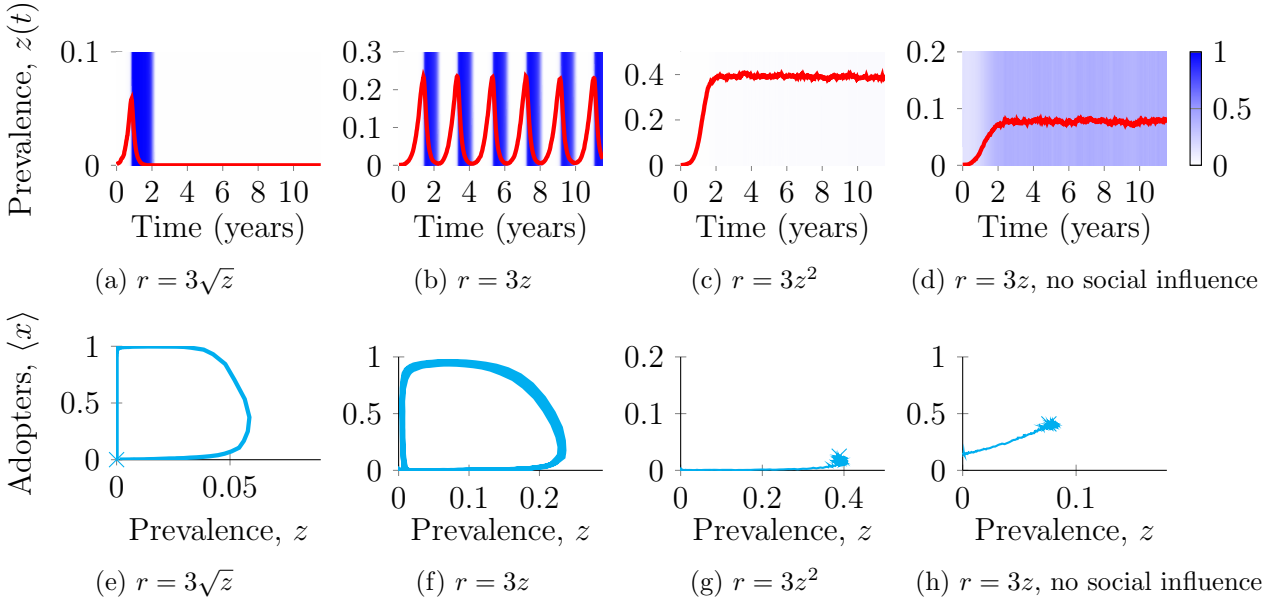


Figure 2: Simulations of the SIS model. In (a)–(d), we show the time-evolution of the epidemic prevalence  $z(t)$  (red) and the fraction of adopters of self-protections  $\langle x(t) \rangle := \frac{1}{n} \sum_{i \in \mathcal{V}} x_i(t)$  (intensity of the blue bands). In (e)–(h), we show the corresponding trajectories on the phase-space. Panels refer to different risk perceptions  $r(z)$ , as detailed in the sub-captions.

where  $\langle a \rangle := \frac{1}{n} \sum_{i \in \mathcal{V}} a_i$  and  $\langle a^2 \rangle := \frac{1}{n} \sum_{i \in \mathcal{V}} a_i^2$  are the mean and second moment of the activity distribution, respectively (the derivation of Eq. (4) is reported in the Supplemental Material). Note that, when the cost for adopting self-protections grows large,  $c \rightarrow \infty$ , the threshold in Eq. (4) tends to the one of a standard SIS model on ADNs [29].

The threshold in Eq. (4) offers insight into the role of human behavior in the early stages of an epidemic outbreak by establishing conditions under which the disease is immediately eradicated. However, the key novelty of the proposed paradigm lies in the possibility to investigate the interplay between human behavior and epidemic spreading in the long term, when the epidemic actually spreads (i.e., above the epidemic threshold). In this scenario, such a complex interplay may give rise to several interesting and realistic phenomena, such as periodic oscillations and multiple waves, the emergence of endemic diseases, and even behavioral responses leading to the successful eradication of the outbreak. In the following, we execute a numerical study to elucidate such phenomena<sup>1</sup>. Specifically, we combine our co-evolutionary model with the classical SIS and susceptible–infected–recovered (SIR) models, parametrized to reproduce real-world diseases. The SIS model is used to illustrate the large variety of phenomena that the paradigm can reproduce, and to discuss the key role of social influence into determining a collective response, confirming recent empirical evidence from the social psychology literature [10]. The SIR model is utilized to show that our model can reproduce real-world epidemic patterns, and to discuss the design of policy interventions. In all the simulations, we fix  $n = 20,000$  individuals (20 of them initially infected). The influence layer is modeled through a Watts–Strogatz small-world network [38] with average degree 8 and rewiring probability 1/8. The contact layer is generated through an ADN with power-law distributed activities  $a_i$  with a negative exponent  $-2.09$ , as in [39], and lower cutoff at  $a_{\min} = 0.1$ . Further details and simulations with other distributions are reported in the Supplemental Material.

We simulate an SIS model calibrated on gonorrhea [40] ( $\lambda = 0.3626$ ,  $\mu = 0.1185$ ,  $m = 1$ , and weekly time-steps, see Supplemental Material), by fixing an immediate cost of  $c = 0.3$  with no accumulation  $\gamma = 0$  and assuming that no policy interventions are enacted ( $u(t) = 0$ ,  $\forall t \geq 0$ ). In Figs. 2a–2c, we consider three scenarios with progressively less cautious populations ( $r(z) = 3\sqrt{z}$ ,  $r(z) = 3z$ , and  $r(z) = 3z^2$ , respectively, see Supplemental Information). We observe that this shift

<sup>1</sup>The code is available at <https://github.com/lzino90/behavior>.

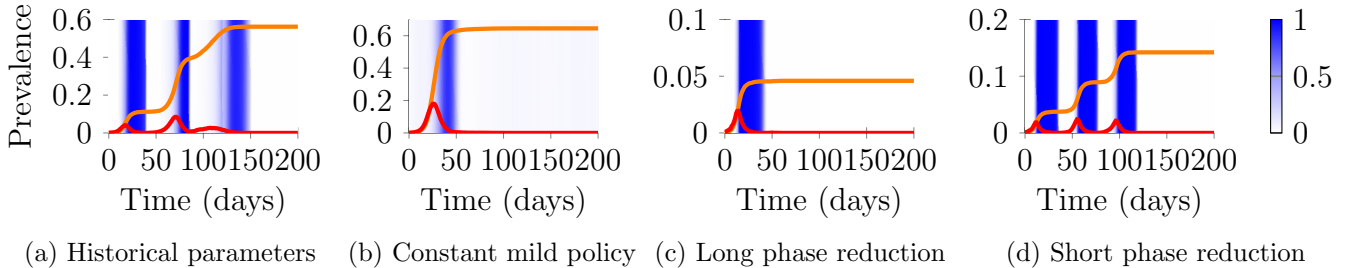


Figure 3: Simulations of the SIR model. Temporal evolution of the epidemic prevalence  $z(t)$  (red), recovered  $R(t) := \frac{1}{n}|\{i : y_i(t) = R\}|$  (orange), and fraction of adopters of self-protections  $\langle x(t) \rangle$  (intensity of the blue vertical bars) with (a) historical parameters of the 1918–19 Spanish flu pandemic [41, 42]; (b) a mild and constant intervention; (c) a severe intervention with a long phased reduction period; and (d) a very severe intervention with a short phased reduction period.

in risk perception causes not only a quantitative shift in the epidemic dynamics, similar to most awareness-based models [5, 6], but more importantly, qualitatively changes the salient phenomena. In fact, the phenomena spans from a prompt and sustained collective response that leads to fast eradication of the disease (in Fig. 2e, the trajectory rapidly reaches the disease-free manifold  $z = 0$ ), to periodic oscillations both in the epidemic prevalence and in the behavioral response (Figs. 2b and 2f), and finally to a partial behavioral response, resulting in the emergence of a meta-stable endemic equilibrium (Figs. 2c and 2g).

In the scenario depicted above, the risk perception function determines a critical prevalence  $z^* = \min\{z : r(z) > 1 + c\}$ , such that  $z(t) > z^*$  implies that the payoff for adopting self-protections is larger than for not adopting them ( $\pi_i^1(t) > \pi_i^0(t)$ ), for any individual, irrespective of the behavior of others. With  $r(z) = 3\sqrt{z}$ , the critical prevalence is  $z^* \approx 18\%$ . However, as can be observed in Fig. 2e, social influence causes individuals to rapidly and widely adopt self-protective behaviors at a much earlier prevalence of  $z \approx 6\%$ , highlighting the key role played by social influence toward facilitating the emergence of collective behavioral patterns and, in this instance, helping in the fast eradication of the disease.

We further investigate the role of social influence by simulating the model in its absence (i.e., removing the first term in Eqs. (2a)–(2b)). Our findings support the intuition that social influence is key to ensure collective population responses, which are in turn crucial for the successful eradication of the disease (Fig. 2a) and the emergence of periodic oscillations (Fig. 2b). In fact, in the absence of social influence, the system shows a less rich range of behaviors, whereby a partial behavioral response always leads to the convergence to an endemic equilibrium (Figs. 2d and 2h are obtained with the parameters of Fig. 2b without social influence; simulations corresponding to Figs. 2a and 2c are reported in the Supplemental Material).

We further elucidate the potentialities of our behavioral paradigm by combining it with an SIR model. In the SIR model, the *removed* ( $R$ ) health state is added to  $\mathcal{A}$  to represent immunized individuals after recovery (or death), and the system is governed by Eq. (3) and  $\mathbb{P}[y_i(t+1) = R | y_i(t) = I] = \mu$ . The model is calibrated on the 1918–19 Spanish flu [41, 43] ( $\lambda = 0.066$ ,  $\mu = 0.2164$ ,  $m = 13$ , and daily time-steps, see Supplemental Material). In particular, we set a risk perception function that increases slowly,  $r = 3z^2$  (associated with the initial suppression of news about the flu [44]), and policy interventions are set to mimic historical lockdowns ( $u(t) = 0.5$  when 1% of the population is infected, and held constant for  $T_a = 28$  days [42]). For airborne diseases like Spanish flu, self-protective behaviors entail physical distancing and closures of economic activities, which often yield an accumulation of psychological distress and economic losses [12, 36, 45]. Accordingly, we set  $c = 0.1$  and  $\gamma = 0.9$  (see Supplemental Material). Figure 3a shows that our paradigm is able to qualitatively reproduce the historical epidemic pattern, which witnessed a resurgent pandemic with three waves that includes a massive second wave [41, 42].

We utilize this example to discuss the design of policy interventions. First, from Fig. 3b, we observe that mild policy interventions, even if indefinite in duration ( $u(t) = 0.4, \forall t \geq 0$ ), may not be sufficient to ensure a timely and collective response, resulting in a massive outbreak that reaches more than 60% of the population. Next, we consider two scenarios with severe but shorter policy interventions, followed by a linear phased reduction (Figs. 3c and 3d); in the first scenario, the policy is less severe ( $u(t) = 0.6$  vs.  $u(t) = 0.8$  for 21 days), but the reduction period is longer (42 vs. 21 days)<sup>2</sup>. Comparing the two scenarios, we conclude that, provided that the initial policy interventions are sufficiently severe to ensure collective adoption of self-protections (thus avoiding the scenario shown in Fig. 3b), the successful eradication of the disease depends primarily on a sufficiently long phased reduction period. This avoids the multiple waves and subsequent lockdowns that would increase both the death toll and the total social-economic cost. The latter point is consistent with recent observations on the duration of policy interventions and their gradual uplifting for the COVID-19 pandemic [46]. Consistent with the SIS results, the SIR outcomes underline the key role of social influence, which may act as a double-edged sword, providing either a driving force or a retarding force for the collective adoption of self-protections, depending on whether the intervention policies are sufficiently strong.

These simulations illustrate the predictive power of our paradigm, once a proper parametrization and model have been extrapolated from empirical data. In fact, existing approaches typically estimate how infection parameters, associated with the disease dynamics, are explicitly changed due to policy interventions [15]. Generally, this is a difficult task that does not explicitly account for the complexity of human behavior. In contrast, our paradigm leaves the disease dynamics untouched, and allows policy interventions to only influence the decision-making process that determines the behavioral responses, which, in turn, shape the epidemic evolution.

In summary, we proposed a novel and unified individual-level modeling paradigm that captures the co-evolution of disease spreading and collective decision-making at the same time scale. Our framework encapsulates a wide range of time-varying factors that are crucial in decision-making during epidemics, from the initial outbreak to its complete eradication, including government interventions, risk perception, bounded rationality, and social influence. The framework decouples the roles of these factors—which collectively shape the behavioral response to an epidemic outbreak—in an intuitive way, enabling their estimation from epidemiological [47], socio-demographic [43], and communication data [48].

Our methodology is presented as a parsimonious paradigm, adaptable to different epidemic progression models [2, 26] and temporal network interactions [28, 30, 31, 33, 49]. Complex real-world phenomena are reproduced within our unified framework—including periodic oscillations, multiple epidemic waves, and prompt collective response by the population leading to the fast eradication of the disease triggered by endogenous risk perception or exogenous policy interventions. Due to its flexibility, further features of the behavioral response can be directly incorporated in the paradigm, including limited effectiveness of self-protections, delays in the behavioral response, and biased risk perceptions due to imperfect information on the epidemic prevalence. Finally, the combination of the proposed paradigm with more complex and realistic epidemic progression models (e.g., those tailored to COVID-19 [50, 51]) is key to further investigating the features captured by our model (e.g., a latency period before infectiousness may lead to overlapping waves, see the Supplemental Material). This may allow our paradigm to be utilized to predict the behavioral response to real-world epidemic outbreaks and, thus, help public health authorities design effective interventions.

L.Z. and M.C. are supported by the European Research Council (ERC-CoG-771687) and the Netherlands Organization for Scientific Research (NWO-vidi-14134); A.R. by Compagnia di San Paolo and the Italian Ministry of Foreign Affairs and International Cooperation (“Mac2Mic”).

M.Y. and L.Z. contributed equally as leading authors. A.R. and M.C. contributed equally.

---

<sup>2</sup>The total control efforts for the two policies, measured as the sum of  $u(t)$  over the duration of a lockdown, are the same.

## References

- [1] Jay J. Van Bavel et al. Using social and behavioural science to support COVID-19 pandemic response. *Nat. Hum. Behav.*, 4(5):460–471, May 2020.
- [2] R. Pastor-Satorras, C. Castellano, P. Van Mieghem, and A. Vespignani. Epidemic processes in complex networks. *Rev. Mod. Phys.*, 87:925–979, 2015.
- [3] S. Funk, M. Salathé, and V. A. Jansen. Modelling the influence of human behaviour on the spread of infectious diseases: a review. *J. R. Soc. Interface*, 7(50):1247–1256, 2010.
- [4] Nicola Perra, Duygu Balcan, Bruno Gonçalves, and Alessandro Vespignani. Towards a Characterization of Behavior-Disease Models. *PLOS One*, 6(8), 08 2011.
- [5] Faryad Darabi Sahneh, Fahmida N. Chowdhury, and Caterina M. Scoglio. On the existence of a threshold for preventive behavioral responses to suppress epidemic spreading. *Sci. Rep.*, 2(1):632, Sep 2012.
- [6] C. Granell, S. Gómez, and A. Arenas. Dynamical interplay between awareness and epidemic spreading in multiplex networks. *Phys. Rev. Lett.*, 111(12):128701, 2013.
- [7] A. Rizzo, M. Frasca, and M. Porfiri. Effect of individual behavior on epidemic spreading in activity driven networks. *Phys. Rev. E*, 90, 2014.
- [8] Zhen Wang, Michael A. Andrews, Zhi-Xi Wu, Lin Wang, and Chris T. Bauch. Coupled disease–behavior dynamics on complex networks: A review. *Phys. Life Rev.*, 15:1 – 29, 2015.
- [9] Frederik Verelst, Lander Willem, and Philippe Beutels. Behavioural change models for infectious disease transmission: a systematic review (2010-2015). *J. R. Soc. Interface*, 13:20160820, 2016.
- [10] Bahar Tunçgenç, Marwa El Zein, Justin Sulik, Martha Newson, Yi Zhao, Guillaume Dezechache, and Ophelia Deroy. Social influence matters: We follow pandemic guidelines most when our close circle does. *Br. J. Psychol.*, 2021.
- [11] Piero Poletti, Bruno Caprile, Marco Ajelli, Andrea Pugliese, and Stefano Merler. Spontaneous behavioural changes in response to epidemics. *J. Theor. Biol.*, 260(1):31–40, 2009.
- [12] Maria Nicola, Zaid Alsafi, Catrin Sohrabi, Ahmed Kerwan, Ahmed Al-Jabir, Christos Iosifidis, Maliha Agha, and Riaz Agha. The socio-economic implications of the coronavirus pandemic (COVID-19): A review. *Int. J. Surg.*, 78:185–193, June 2020.
- [13] Sansao A. Pedro, Frank T. Ndjomatchoua, Peter Jentsch, Jean M. Tchuenche, Madhur Anand, and Chris T. Bauch. Conditions for a Second Wave of COVID-19 Due to Interactions Between Disease Dynamics and Social Processes. *Front. Phys.*, 8:428, 2020.
- [14] Herbert A. Simon. Bounded rationality in social science: Today and tomorrow. *Mind Soc.*, 1(1):25–39, Mar 2000.
- [15] Nicola Perra. Non-pharmaceutical interventions during the covid-19 pandemic: A review. *Phys. Rep.*, 2021.
- [16] Jocelyne Piret and Guy Boivin. Pandemics throughout history. *Front. Microbiol.*, 11:3594, 2021.
- [17] H. Peyton Young and Shmuel Zamir, editors. *Handbook of Game Theory with Economic Applications*, volume 4. Elsevier, 2015.

- [18] K. M. Ariful Kabir and Jun Tanimoto. Evolutionary game theory modelling to represent the behavioural dynamics of economic shutdowns and shield immunity in the COVID-19 pandemic. *R. Soc. Open Sci.*, 7(9):201095, 2020.
- [19] Jinyu Wei, Li Wang, and Xin Yang. Game analysis on the evolution of COVID-19 epidemic under the prevention and control measures of the government. *PLOS ONE*, 15(10):1–16, 10 2020.
- [20] Chris T. Bauch and David J. D. Earn. Vaccination and the theory of games. *Proc. Natl. Acad. Sci. USA*, 101(36):13391–13394, 2004.
- [21] Feng Fu, Daniel I. Rosenbloom, Long Wang, and Martin A. Nowak. Imitation dynamics of vaccination behaviour on social networks. *Proc. Royal Soc. B*, 278(1702):42–49, 2011.
- [22] Hai-Feng Zhang, Zhi-Xi Wu, Ming Tang, and Ying-Cheng Lai. Effects of behavioral response and vaccination policy on epidemic spreading — an approach based on evolutionary-game dynamics. *Sci. Rep.*, 4(1):5666, Jul 2014.
- [23] Xingru Chen and Feng Fu. Imperfect vaccine and hysteresis. *Proc. Royal Soc. B*, 286(1894):20182406, 2019.
- [24] Sheryl L. Chang, Mahendra Piraveenan, Philippa Pattison, and Mikhail Prokopenko. Game theoretic modelling of infectious disease dynamics and intervention methods: a review. *J. Biol. Dyn.*, 14(1):57–89, 2020.
- [25] Chad R. Wells, Amit Huppert, Meagan C. Fitzpatrick, Abhishek Pandey, Baruch Velan, Burton H. Singer, Chris T. Bauch, and Alison P. Galvani. Prosocial polio vaccination in Israel. *Proc. Natl. Acad. Sci. USA*, 117(23):13138–13144, 2020.
- [26] F. Brauer and C. Castillo-Chavez. *Mathematical models in population biology and epidemiology*. Springer, 2012.
- [27] S. Boccaletti, G. Bianconi, R. Criado, C.I. del Genio, J. Gómez-Gardeñes, M. Romance, I. Sendiña-Nadal, Z. Wang, and M. Zanin. The structure and dynamics of multilayer networks. *Phys. Rep.*, 544(1):1 – 122, 2014.
- [28] P. Holme and J. Saramäki. Temporal networks. *Phys. Rep.*, 519:97–125, 2012.
- [29] N. Perra, B. Gonçalves, R. Pastor-Satorras, and A. Vespignani. Activity driven modeling of time varying networks. *Sci. Rep.*, 2, 2012.
- [30] Petter Holme. Modern temporal network theory: a colloquium. *Eur. Phys. J. B*, 88(9), 2015.
- [31] E. Valdano, L. Ferreri, C. Poletto, and V. Colizza. Analytical computation of the epidemic threshold on temporal networks. *Phys. Rev. X*, 5:021005, 2015.
- [32] Lorenzo Zino, Alessandro Rizzo, and Maurizio Porfiri. Continuous-time discrete-distribution theory for activity-driven networks. *Phys. Rev. Lett.*, 117:228302, 2016.
- [33] Andreas Koher, Hartmut H. K. Lentz, James P. Gleeson, and Philipp Hövel. Contact-based model for epidemic spreading on temporal networks. *Phys. Rev. X*, 9:031017, Aug 2019.
- [34] Lawrence Blume. The Statistical Mechanics of Best-Response Strategy Revision. *Games Econ. Behav.*, 11(2):111–145, 1995.

- [35] Matthew O. Jackson and Yves Zenou. Games on Networks. In *Handbook of Game Theory with Economic Applications*, volume 4, chapter 3, pages 95–163. Elsevier, 2015.
- [36] Jianyin Qiu, Bin Shen, Min Zhao, Zhen Wang, Bin Xie, and Yifeng Xu. A nationwide survey of psychological distress among Chinese people in the COVID-19 epidemic: implications and policy recommendations. *Gen. Psychiatr.*, 33(2):e100213–e100213, Mar 2020.
- [37] P. Van Mieghem, J. Omic, and R. Kooij. Virus spread in networks. *IEEE/ACM Trans. Netw.*, 17(1):1–14, Feb 2009.
- [38] Duncan J. Watts and Steven H. Strogatz. Collective dynamics of ‘small-world’ networks. *Nature*, 393(6684):440–442, Jun 1998.
- [39] William Aiello, Fan Chung, and Linyuan Lu. A random graph model for power law graphs. *Exp. Math.*, 10(1):53–66, 2001.
- [40] JAMES A. Yorke, HERBERT W. Hethcote, and ANNETT Nold. Dynamics and Control of the Transmission of Gonorrhoea. *Sex. Transm. Dis.*, 5(2):51–55, 1978.
- [41] Christina E. Mills, James M. Robins, and Marc Lipsitch. Transmissibility of 1918 pandemic influenza. *Nature*, 432(7019):904–906, Dec 2004.
- [42] Howard Markel, Harvey B. Lipman, J. Alexander Navarro, Alexandra Sloan, Joseph R. Michalsen, Alexandra Minna Stern, and Martin S. Cetron. Nonpharmaceutical Interventions Implemented by US Cities During the 1918-1919 Influenza Pandemic. *JAMA*, 298(6):644–654, 08 2007.
- [43] Joël Mossong, Niel Hens, Mark Jit, Philippe Beutels, Kari Auranen, Rafael Mikolajczyk, Marco Massari, Stefania Salmaso, Gianpaolo Scalia Tomba, Jacco Wallinga, et al. Social Contacts and Mixing Patterns Relevant to the Spread of Infectious Diseases. *PLOS Med.*, 5(3), 03 2008.
- [44] John M. Barry. Pandemics: avoiding the mistakes of 1918. *Nature*, 459(7245):324–325, May 2009.
- [45] Alexander W. Bartik, Marianne Bertrand, Zoe Cullen, Edward L. Glaeser, Michael Luca, and Christopher Stanton. The impact of COVID-19 on small business outcomes and expectations. *Proc. Natl. Acad. Sci. USA*, 117(30):17656–17666, 2020.
- [46] Leonardo López and Xavier Rodó. The end of social confinement and COVID-19 re-emergence risk. *Nat. Hum. Behav.*, 4(7):746–755, Jul 2020.
- [47] Sarah Cobey. Modeling infectious disease dynamics. *Science*, 368(6492):713–714, 2020.
- [48] Nuria Oliver, Bruno Lepri, Harald Sterly, Renaud Lambiotte, Sébastien Deletaille, Marco De Nadai, Emmanuel Letouzé, Albert Ali Salah, Richard Benjamins, Ciro Cattuto, et al. Mobile phone data for informing public health actions across the covid-19 pandemic life cycle. *Sci. Adv.*, 6(23), 2020.
- [49] L. Zino, A. Rizzo, and M. Porfiri. Modeling memory effects in activity-driven networks. *SIAM J. Appl. Dyn. Syst.*, 17(4):2830–2854, 2018.
- [50] Ernesto Estrada. COVID-19 and SARS-CoV-2. Modeling the present, looking at the future. *Phys. Rep.*, 869:1–51, 2020.

- [51] Alex Arenas, Wesley Cota, Jesús Gómez-Gardeñes, Sergio Gómez, Clara Granell, Joan T. Matamalas, David Soriano-Paños, and Benjamin Steinegger. Modeling the spatiotemporal epidemic spreading of covid-19 and the impact of mobility and social distancing interventions. *Phys. Rev. X*, 10:041055, Dec 2020.

# SUPPLEMENTAL MATERIAL

## Game-theoretic modeling of collective decision-making during epidemics

Mengbin Ye<sup>1</sup>, Lorenzo Zino<sup>2</sup>, Alessandro Rizzo<sup>3,\*</sup> and Ming Cao<sup>2</sup>

<sup>1</sup> *Optus-Curtin Centre of Excellence in Artificial Intelligence, Curtin University, Perth, Australia*

<sup>2</sup> *Faculty of Science and Engineering, University of Groningen, Groningen, Netherlands*

<sup>3</sup> *Dipartimento di Elettronica e Telecomunicazioni, Politecnico di Torino, 10129 Torino, Italy*

(Dated: May 13, 2021)

### DETAILS OF THE NETWORK STRUCTURE

The two-layered network structure with a static influence layer and a time-varying physical contact layer, illustrated in Supplemental Fig. S1a, is motivated by the observation that social relationships (e.g. between family members, friends, colleagues) typically change at a much slower pace than that of epidemic processes and thus can be assumed constant, while the network of physical contacts evolves at a time-scale comparable with the spread of the disease [1].

In our analytical computations and numerical simulations, the contact layer is modeled using an activity-driven network (ADN) [2]. ADNs have emerged as a powerful paradigm to study the dynamical co-evolution of i) the network structure, and ii) the process unfolding at each node. ADNs have found successful application in mathematical epidemiology [3]. The network formation process acts as follows. At each discrete time instant  $t$ , with probability  $a_i$ , individual  $i$  activates and generates a fixed number of contacts  $m \geq 1$  with other individuals chosen uniformly at random in the population. These contacts are added to the link set  $\mathcal{E}_C(t)$ , contribute to the epidemic process, and are then removed before the next discrete time instant and the next activation of individuals. Despite their simplicity, which enables rigorous analytical treatment and fast numerical simulations [2, 4], ADNs can capture important features of complexity that characterize real-world networks and are amenable to analytically-tractable extensions to include further features [1]. Importantly, the proposed modeling paradigm can also use other time-varying network models [5–7].

### DETAILS OF THE SIR MODEL

In the SIR model, whose schematic is illustrated in Supplemental Fig. S1b, individuals may have three different health states: they can be susceptible to the disease ( $S$ ); infected ( $I$ ); or removed ( $R$ ), accounting for both recoveries

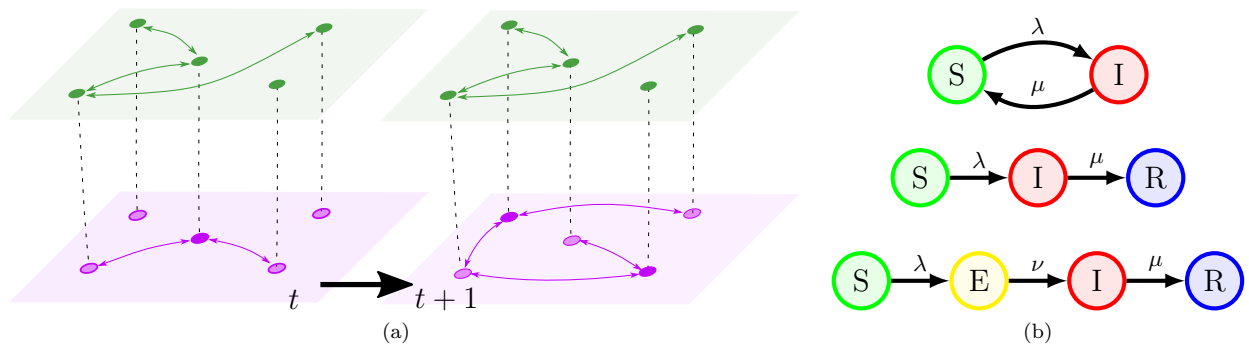


FIG. S1: Illustration of the network model and the epidemic progression. In (a), two time-steps in the two-layer network representation. The upper layer (green) shows influences, the lower layer (violet) physical contacts. In (b), schematics of the state transitions of the SIS model (above), of the SIR model (middle), and of the SEIR model (below). The constants  $\lambda$  and  $\mu$  indicate transition probabilities.

\* Also at Office of Innovation, New York University Tandon School of Engineering, 11201 Brooklyn NY, USA

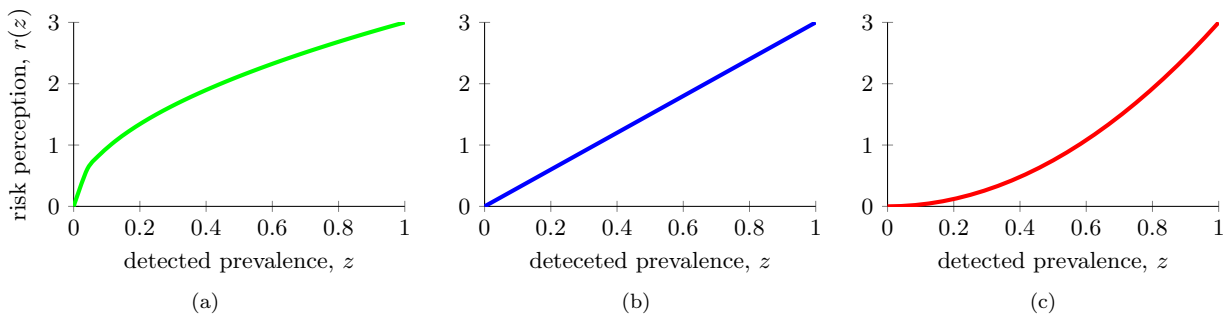


FIG. S2: The three different risk perception function  $r(z)$  used in the simulations.

and deaths. The disease spreads as for the SIS model, i.e.,

$$\mathbb{P}[y_i(t+1) = I | x_i(t) = S] = (1 - x_i(t)) \left(1 - (1 - \lambda)^{N_i(t)}\right), \quad (1)$$

where

$$N_i(t) = |\{j \in \mathcal{V} : (i, j) \in \mathcal{E}_C(t), y_j(t) = I\}| \quad (2)$$

is the number of infectious individuals that have a link with node  $i$  at time  $t$  on the contact layer. The recovery process is governed by the same probabilistic rule as for the SIS model but, once recovered, individuals become removed ( $R$ ) and cannot be infected again, i.e.,

$$\mathbb{P}[y_i(t+1) = R | y_i(t) = I] = \mu. \quad (3)$$

#### DETAILS OF THE DECISION-MAKING MECHANISM

Here, we provide some additional details and comments on the decision-making mechanism.

**Rationality.** The parameter  $\beta \in [0, \infty)$  and the log-linear learning dynamics in (5) together model bounded rationality in an individual's decision-making process. We have assumed for simplicity that  $\beta$  is homogeneous among all individuals in this work, but this is easily generalizable to a heterogeneous  $\beta_i$  distribution. Notice that if  $\beta = 0$ , individuals make decisions uniformly at random, while for  $\beta \rightarrow \infty$ , individuals apply perfect rationality to select the behavior with highest payoff. This best-response behavior is myopic, i.e., individuals do not look forward in time to optimize a sequence of decisions. Myopic behavior is reasonable given the uncertain nature of a long-lasting epidemic.

**Risk perception function.** The risk perception function is a monotonic nondecreasing function of  $z(t)$ , capturing the fear of being infected, which rises as the number of infectious individuals increase. In its simplest formulation (which is adopted in the case studies presented in this letter), it can be assumed to be a power function

$$r(z) = kz^\alpha, \quad (4)$$

with  $k > 0$  and  $\alpha > 0$ . Specifically,  $\alpha \in (0, 1)$  models cautious populations, where a small initial outbreak causes a large increase in the risk perception. The case  $\alpha = 1$  captures a population whose reaction grows linearly with the epidemic prevalence observe. On the contrary,  $\alpha > 1$  captures populations that underestimate the risk, and the epidemic prevalence must be large before the risk perception plays an important role in the decision-making process. The constant  $k$  is a scaling constant. In the simulations in the letter, we considered three different functions as archetypes of three different scenarios: a cautious population ( $\alpha = 1/2$ ), a population with reaction proportional to the epidemic prevalence ( $\alpha = 1$ ), and a slow reacting population ( $\alpha = 2$ ). These three functions are illustrated in Supplemental Fig. S2. In all three cases we set  $k = 3$ .

We remark that the risk perception (as well as the cost of self-protection) is endogenous to each individual, different from the policy intervention  $u(t)$ , which is exogenous and from the social influence, which is determined by the interactions on the influence layer.

Note that in this work, we have for simplicity defined the detected prevalence  $z(t) = \frac{1}{n} |\{i : y_i(t) = I\}|$  as the fraction of individuals who are infectious, i.e., in the health state  $I$ . For practical studies, and depending on the disease,  $z(t)$  may be defined with more complexity to reflect under-reporting of testing or delays in test results, visibility of asymptomatic vs. symptomatic individuals (as opposed to exposed vs. infectious states), differing prevalence due to spatial structures, etc.

## DERIVATION OF THE EPIDEMIC THRESHOLD FOR THE SIS MODEL

In the absence of cumulative frustration and for a fully mixed influence layer, we observe that

$$\mathbb{P}[x_i(t+1) = 0] = \frac{\exp\{\beta\pi_i(0)\}}{\exp\{\beta\pi_i^0(t)\} + \exp\{\beta\pi_i^1(t)\}} \quad (5)$$

has the same expression for all the individuals (nodes). In fact, if we define  $\bar{x}(z)$  as the probability that a generic node adopts self-protective behaviors when the epidemic prevalence is equal to  $z$ , then, according to the strong law of large numbers,  $\pi_i^0(t) = 1 - \bar{x}(z) - u(t) = 1 - \bar{x}(z) - \bar{u}$  (since the control is assumed to be a constant function) and  $\pi_i^1(t) = \bar{x}(z) + r(z) - c$ , which are independent of  $i$ . In a mean-field approach [8], we define  $\theta(t) = \frac{1}{n} \sum_{i: y_i(t)=I} a_i$  as the average activity of infected nodes and  $z_i(t) = \mathbb{P}[y_i(t) = I]$ . Due to the strong law of large numbers, in the limit of large-scale systems  $n \rightarrow \infty$ ,  $z(t) = \frac{1}{n} \sum_{i=1}^n z_i(t)$  and  $\theta(t) = \frac{1}{n} \sum_{i=1}^n a_i z_i(t)$ . Hence, from the mean-field evolution of  $z_i(t)$ , given by

$$z_i(t+1) = z_i(t) - \mu z_i(t) + m\lambda(1 - z_i(t))(1 - \bar{x}(z(t)))a_i z_i(t) + (1 - z_i(t))(1 - \bar{x}(z(t)))\lambda m\theta(t), \quad (6)$$

we determine the following system of difference equations for the epidemic prevalence and the average activity of infected individuals, linearized about the disease-free equilibrium ( $z = 0, \theta = 0$ ):

$$\begin{aligned} z(t+1) &= z(t) - \mu z(t) + m\lambda\langle a \rangle z(t)(1 - \bar{x}(0)) + m\lambda(1 - \bar{x}(0))\theta(t) \\ \theta(t+1) &= \theta(t) - \mu\theta(t) + m\lambda\langle a^2 \rangle z(t)(1 - \bar{x}(0)) + m\lambda\langle a \rangle(1 - \bar{x}(0))\theta(t), \end{aligned} \quad (7)$$

where  $\langle a \rangle$  and  $\langle a^2 \rangle$  are the average and second moment of the activity distribution, respectively.

From standard theory on the stability of discrete-time linear time-invariant systems [9], the origin is stable if

$$\frac{\lambda}{\mu} < \frac{1}{m(\langle a \rangle + \sqrt{\langle a^2 \rangle})(1 - \bar{x}(0))}. \quad (8)$$

In fully-mixed influence layers, the probability for an individual to adopt self-protective behaviors  $\bar{x}(z)$  can be derived by substituting  $\pi_i(0) = 1 - \bar{x}(z) - \bar{u}$  and  $\pi_i(1) = \bar{x}(z) + r(z) - c$  into (5), obtaining the equilibrium equation:

$$\bar{x} = \frac{e^{\beta(\bar{x}-c+r(z))}}{e^{\beta(\bar{x}-c+r(z))} + e^{\beta(1-\bar{x}-\bar{u})}}. \quad (9)$$

Even though it is not possible to derive a closed-form solution, we observe that at the inception of the epidemic outbreak,  $x_i(0) = 0$  for all individuals and, for sufficiently small values of  $\bar{u}$  (i.e.,  $\bar{u} \ll 1 + c$ ), in the early stages it is verified that  $\pi_i^0(t) > \pi_i^1(t)$ . Hence, if the rationality  $\beta$  is sufficiently large, the equilibrium  $\bar{x}$  is close to 0 and can be approximated by Taylor-expanding the right-hand side of the equation, obtaining

$$\bar{x}(z) \approx \frac{e^{\beta(-c+r(z))}}{e^{\beta(1-\bar{u})} + (1 - \beta)e^{\beta(-c+r(z))}}. \quad (10)$$

## NETWORK PARAMETERS OF THE SIMULATIONS

In all the simulations, we consider  $n = 20,000$  individuals (20 of them initially infected) connected on the influence layer through a Watts–Strogatz small-world network, which captures many features of real-world influence networks, including a clustered structure and the presence of long-range interactions [10]. We set an average degree 8 and rewiring probability 1/8, so that each node has on average 1 long-range interaction.

In the simulations in the main article, the contact layer is generated following an ADN with power-law distributed activities  $a_i$ , which is a standard assumption for ADNs [2]. Note that while the activity rates  $a_i$  are power-law distributed, at each time-step, the node degree distribution does not follow a power-law, and are instead determined by the homogeneous parameter  $m$  capturing the bounded number of interactions that each individual can have per unit time-step. Specifically, we set the negative exponent equal to  $-2.09$ , as in [11], and lower cutoff at  $a_{\min} = 0.1$ . We set  $m = 1$  interactions per active node for the SIS model (calibrated on gonorrhoea) and  $m = 13$  for the SIR model (calibrated on Spanish flu), based on [12]. Simulations with other activity distributions (namely, a log-normal and a Weibull distribution) are reported to demonstrate the robustness of our framework in Supplemental Fig. S3.

## EPIDEMIC PARAMETERS OF THE SIMULATIONS

We perform our numerical simulations using two classical epidemic models: the SIS and the SIR models. The SIS is calibrated on gonorrhea, which is a sexually transmitted disease characterized by negligible protective immunity after recovery and negligible latency period (individuals are infectious on average the day after contagion) [13, 14]. The SIR model is parametrized based on Spanish flu pandemic, which is characterized by a short latency period (individuals are infectious on average after 1–2 days from the contagion [15]) that can be neglected and by protective immunity gained after recovery [15].

The epidemic parameters are set from epidemiological data. Specifically, reliable estimations of the time from infection to recovery  $\tau$  are available [14, 15]. Similar to Prem et al. [16], from these data we define

$$\mu = 1 - \exp\left(-\frac{1}{\tau}\right). \quad (11)$$

Finally, the parameter  $\lambda$  is obtained from available estimations of the basic reproduction number  $R_0$  for the two diseases [14, 15]. The basic reproduction number is defined as the average number of secondary infections produced by an infected individual in a population where everyone is susceptible. Hence, given that  $\tau$  is the average time that an individual is infectious, assuming independence between the time an individual is infectious and their activity, we compute

$$R_0 = \frac{1}{n} \sum_{i \in \mathcal{V}} (a_i + \langle a \rangle) m \lambda \tau = 2 \langle a \rangle m \lambda \tau, \quad (12)$$

which implies

$$\lambda = \frac{R_0}{2m \langle a \rangle \tau}. \quad (13)$$

The epidemic parameters computed using this procedure are the following.

- **SIS Model.** From  $\tau = 55$  days and  $R_0 = 1.6$ , we find  $\lambda = 0.3626$  and  $\mu = 0.1195$ , where the time unit is a week.
- **SIR Model.** From  $\tau = 4.1$  days and  $R_0 = 2$ , we obtain  $\lambda = 0.066$  and  $\mu = 0.2164$ , where the time unit is a day.

## DECISION-MAKING PARAMETERS OF THE SIMULATIONS

We set a common level of rationality  $\beta = 6$  in all simulations, which captures a moderate level of rationality so that individuals tend to maximize their payoff, but always have a small but nonnegligible probability of adopting the behavior with the lower payoff. Before detailing the parameters used in the three case studies, we provide a brief discussion on the relative order of magnitude between the model parameters, which guided our choices.

The decision-making process is based on the comparison between the two payoff functions, that is,

$$\pi_i(0) := \frac{1}{d_i} \sum_{j:(i,j) \in \mathcal{E}_I} (1 - x_j(t)) - u(t), \quad (14a)$$

$$\pi_i(1) := \frac{1}{d_i} \sum_{j:(i,j) \in \mathcal{E}_I} x_j(t) + r(z(t)) - f_i(t). \quad (14b)$$

The contribution of social influence to the payoff is always bounded between 0 and 1. Hence, social influence is significant if the other terms do not have a higher order of magnitude. Consequently, policy interventions  $u(t) > 1$  can be considered severe, since their effect is predominant with respect to social influence, while policies with  $u(t) < 1$  are milder. The cost of self-protective behaviors consists of two terms: the immediate cost per unit-time  $c$  and the accumulation factor  $\gamma$ . Small values of  $c$  become negligible in the decision making process, while, to avoid the immediate cost dominating the other terms, we should assume  $c < 1$ . The accumulation factor  $\gamma$  captures the cost for continued periods in which an individual adopts self-protective behaviors. To model a nonnegligible effect of the

accumulation of socio-economic costs, we should guarantee that over long periods in which an individual consistently adopts self-protective behaviors, the frustration function saturates to a value comparable to the other terms. This can be achieved by imposing that

$$\lim_{t \rightarrow \infty} c + \sum_{s=1}^t \gamma^s c = \frac{c}{1-\gamma} \approx 1, \quad (15)$$

yielding  $c + \gamma \approx 1$  (note, the above equality was obtained using the geometric series). Specifically, values of  $\gamma > 1 - c$  guarantees that self-protective behaviors are eventually dismissed, after the complete eradication of the disease or the policy intervention is switched off. We use the risk perception function  $r(t) = kz^\alpha$  proposed in (4) with  $\alpha = 1/2$  for cautious populations,  $\alpha = 1$  to model proportional reactions, and  $\alpha = 2$  for slow reacting populations. As discussed in the main article, the risk perception function determines a critical epidemic prevalence  $z^* = \min\{z : r(z) > 1 + c\}$  that triggers the adoption of self-protective behaviors even in the absence of interventions (in the presence of accumulation, the immediate cost  $c$  in the expression of  $z^*$  is substituted by its saturation value from (15), being  $c/(1 - \gamma)$ ). We observe that risk perception becomes nonnegligible if  $k > 1 + \frac{c}{1-\gamma}$ . To keep consistency throughout our simulations, we set  $k = 3$ , which is a value that verifies the condition above for all the choices of parameters  $c$  and  $\gamma$  we make in the simulations.

The decision-making parameters used for the two models are detailed in the following.

- **SIS model.** We assume that the accumulation is negligible for gonorrhea (where the use of protections has an immediate cost that typically does not accumulate, such as protective sexual barriers). Hence, for all three simulations, we fix the immediate cost to  $c = 0.3$  and the accumulation factor  $\gamma = 0$ . No policy intervention is set, with  $u(t) = 0$  for all  $t \geq 0$ . In the three simulations, we test three different risk perception functions. Specifically, we consider a cautious population with  $r(z) = 3\sqrt{z}$  in Figs. 2a and 2e in the letter, a population with a proportional reaction,  $r(z) = 3z$  in Figs. 2b, 2d, 2f, and 2h in the letter, and a population slow to react with  $r(z) = 3z^2$  in Figs. 2c and 2g in the letter.
- **SIR model.** Self-protective behaviors involve social distancing and closures of economic activities, which has been shown to typically yield an accumulation of psychological distress and economic losses [17–19]. Hence, we assume a high accumulation factor  $\gamma = 0.9$  and we fix  $c = 0.1$ , in light of our discussion above. To capture the slow reaction of the population due to the initial suppression of information (to keep morale up during World War I) [20, 21], we set  $r(z) = 3z^2$ . To further mirror real-world interventions by public authorities, in Fig. 3a in the letter, we set an initial intervention level equal to  $u(0) = 0$ , which switches to  $u(t) = \bar{u} = 0.5$  once 1% of the population is infected and then remains active for 28 days before being turned off again, consistent with [20]. Then, we consider three different scenarios of intervention policies. In Fig. 3b in the letter, we set a constant mild level of interventions  $u(t) = 0.4$ , for all  $t \geq 0$ . In the other two scenarios, we set  $u(0) = 0$ . Then, in Fig. 3c in the letter, severe policies ( $u(t) = 0.6$ ) are implemented for 21 days after reaching 1% of infections, after which  $u(t)$  is linearly reduced to  $u(t) = 0$  over 42 time-steps. In the second scenario (Fig. 3d in the letter), more severe policies ( $u(t) = 0.8$ ) are implemented for the same period of 21 time-steps, after which  $u(t)$  is linearly reduced to  $u(t) = 0$  over a shorter time-window of 21 time-steps. Note that we select the intensity of policy interventions and the duration of the phased reduction to ensure that the cumulative intervention effort,  $\sum_t u(t)$ , over the duration of a lockdown, is equal to 25.2 in both scenarios.

## SUSCEPTIBLE–EXPOSED–INFECTIOUS–REMOVED (SEIR) MODEL

In the SEIR model (illustrated in Supplemental Fig. S1b), individuals may have four different health states  $y_i(t)$ : they can be susceptible to the disease ( $S$ ); exposed ( $E$ ), i.e., already infected but noninfectious to other individuals; infectious ( $I$ ); or removed ( $R$ ), accounting for both recoveries and deaths. The disease spreads in a manner similar to the SIS and SIR models, i.e., through a link on the contact layer between a susceptible individual ( $S$ ) and an infectious one ( $I$ ). Different from the other two models, after contagion, individuals becomes exposed ( $E$ ) but noninfectious with a latency period before transitioning to the infectious state ( $I$ ). The disease propagates through contacts, each one independent of the others, yielding

$$\mathbb{P}[y_i(t+1) = E | y_i(t) = S] = (1 - x_i(t)) \left(1 - (1 - \lambda)^{N_i(t)}\right), \quad (16)$$

where  $N_i(t) = |\{j \in \mathcal{V} : (i, j) \in \mathcal{E}_C(t), y_j(t) = I\}|$ . Note that exposed individuals are assumed to be not detected.

Beside the contagion, two other mechanisms govern the epidemic process: the progression to becoming infectious, and the recovery process. Specifically, at each time-step  $t$ , every individual  $i$  that is exposed ( $E$ ) has probability  $\nu \in (0, 1]$  to become infectious, independent of the others, giving

$$\mathbb{P}[y_i(t+1) = I \mid y_i(t) = E] = \nu. \quad (17)$$

Then, infectious individuals have probability  $\mu \in (0, 1]$  to recover, independent of the others, giving

$$\mathbb{P}[y_i(t+1) = R \mid y_i(t) = I] = \mu. \quad (18)$$

Similar to the SIR model, once removed, individuals are immunized (or deceased) and cannot be infected again.

We calibrate the SEIR model to the ongoing COVID-19 pandemic [16]. Following the same procedure explained in the above, we define

$$\nu = 1 - \exp\left(-\frac{1}{\tau_E}\right) = 1 - \exp\left(-\frac{1}{6.4}\right) = 0.1447, \quad \text{and} \quad \mu = 1 - \exp\left(-\frac{1}{\tau_I}\right) = 1 - \exp\left(-\frac{1}{5}\right) = 0.1813, \quad (19)$$

where  $\tau_E = 6.4$  days and  $\tau_I = 5$  days are reliable estimations of the time from contagion to becoming infectious and the time from the beginning of the infectiousness period to recovery, respectively [16]. The per-contact infection rate  $\lambda$  is computed from  $R_0 = 2.2$  (computed for the original strain [16]), as

$$\lambda = \frac{R_0}{2m\langle a \rangle \tau_I} = 0.06. \quad (20)$$

Similar as we did for the Spanish flu, we assume that accumulation is nonnegligible by setting  $\gamma = 0.75$ . Note that we select a smaller value of  $\gamma$  than the one used for Spanish flu to capture how development in information and communications technologies has helped alleviate the negative impact of extended lockdown policies during COVID-19 outbreak. In view of the observations above, we fix  $c = 0.3$ . We consider a scenario in which individuals are slow to perceive COVID-19 as a real threat ( $r(z) = 3z^2$ ), as happened in many countries including the UK and US during the first months of the pandemic [22]. We start with  $u(0) = 0$ , and then set the intervention as  $u(t) = 0.7$  when 1% of the population is infectious, which is then turned off if 14 consecutive days pass with  $z(t) = 0$ . The following figure shows the emergence of two massive overlapping waves.

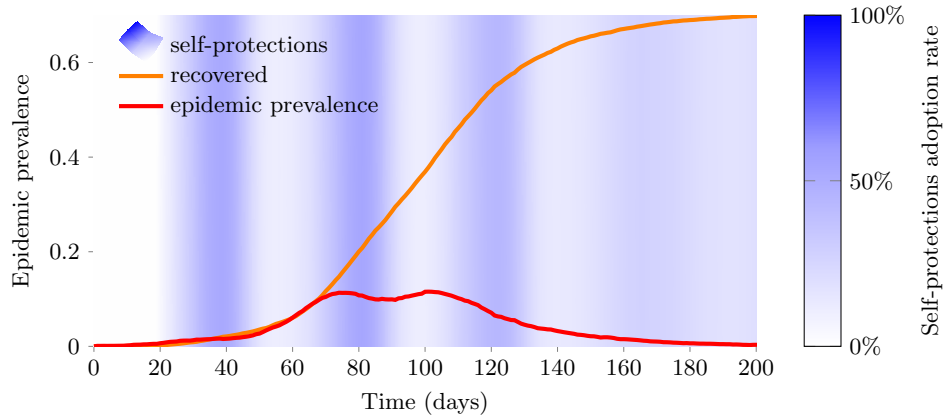


FIG. S3: Simulation of the SEIR model calibrated on COVID-19. The figure shows the infections (red), cumulative removed individuals (orange), and fraction of adopters of self-protective behaviors (intensity of the blue vertical bands). A mild policy intervention and accumulating frustration results in sporadic and noncollective adoption of self-protection, and thus two massive epidemic waves that overlap, followed by a long tail.

## SUPPLEMENTAL SIMULATIONS

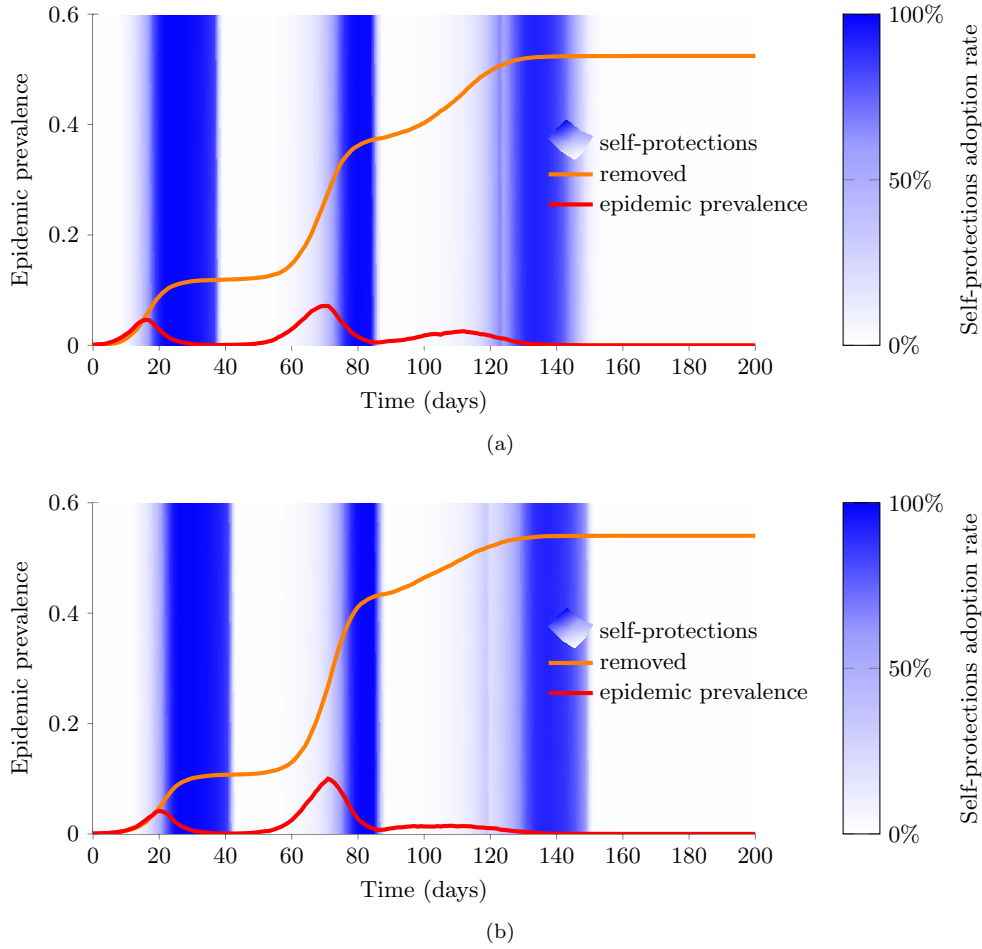
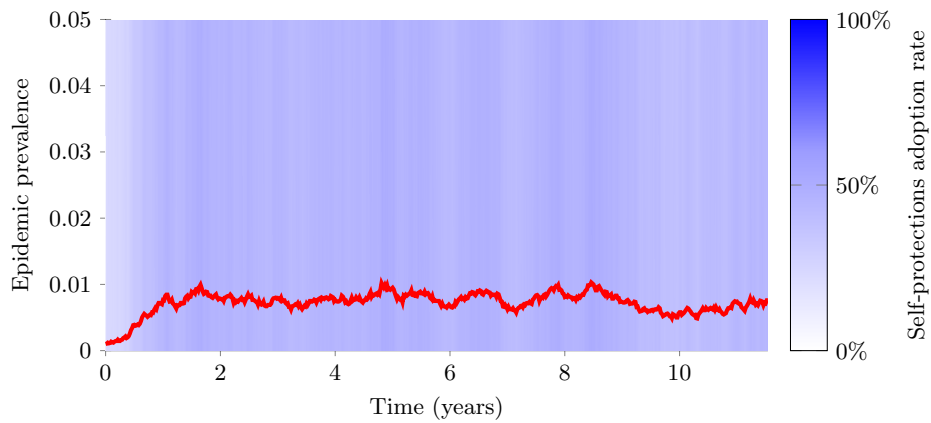
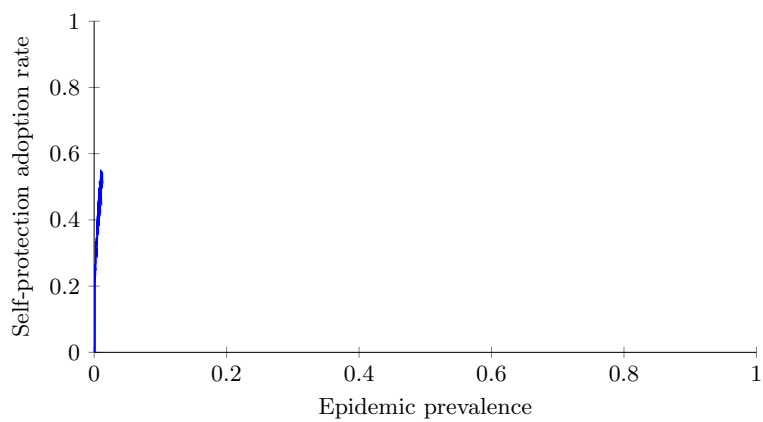


FIG. S4: Robustness against different activity distributions. We show the same simulation as that corresponding to Fig. 3a in the main article in a scenario where the activities are (a) log-normally-distributed ( $\mu = -1.4457$ ,  $\sigma = 0.5987$ ) and (b) Weibull-distributed ( $\lambda = 0.3135$ ,  $k = 1.5555$ ), respectively, with the same mean ( $\langle a \rangle = 0.2818$ ) and second moment ( $\langle a^2 \rangle = 0.1137$ ) as the power-law distribution in Fig. 3a in the main article. In both scenarios, parameters of the distribution are selected to ensure that the average and variance of the distributions equal to the ones of the power-law distribution used in Fig. 3a in the main article. The figures show the prevalence of Spanish flu infections (red curve) and cumulative infections (orange curve) as a function of time as predicted by an SIR model in combination with the co-evolution paradigm. The color intensity of the blue vertical bands represents the fraction of adopters of self-protective behaviors. The simulation results are qualitatively consistent with the one obtained with a power-law distribution for the activities in Fig. 3a in the main article.



(a)



(b)

FIG. S5: Simulation of the SIS model in Fig. 2a, in the absence of social influence. In (a) we show the epidemic prevalence  $z(t)$  (red) and fraction of adopters  $\langle x(t) \rangle := \frac{1}{n} \sum_{i \in \mathcal{V}} x_i(t)$  (color intensity of the blue vertical bands); in (b), we show the corresponding trajectories on the phase space. The risk perception function is  $r(z) = 3\sqrt{z}$ . We observe that, in the absence of social influence, the system converges to an endemic equilibrium with a fraction of population that is adopting self-protections.

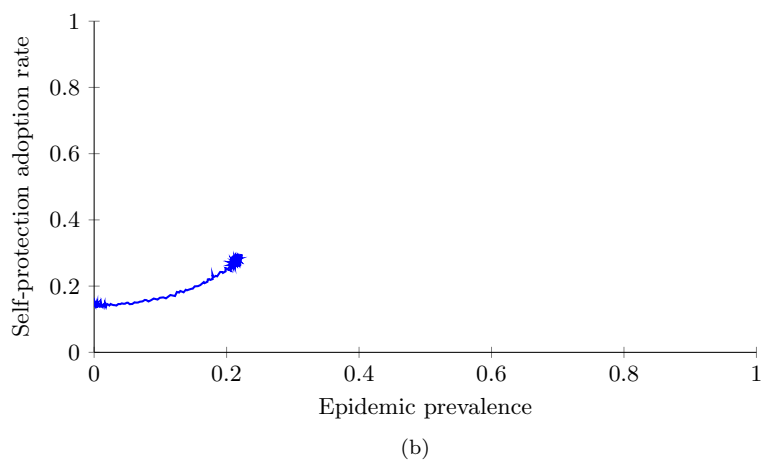
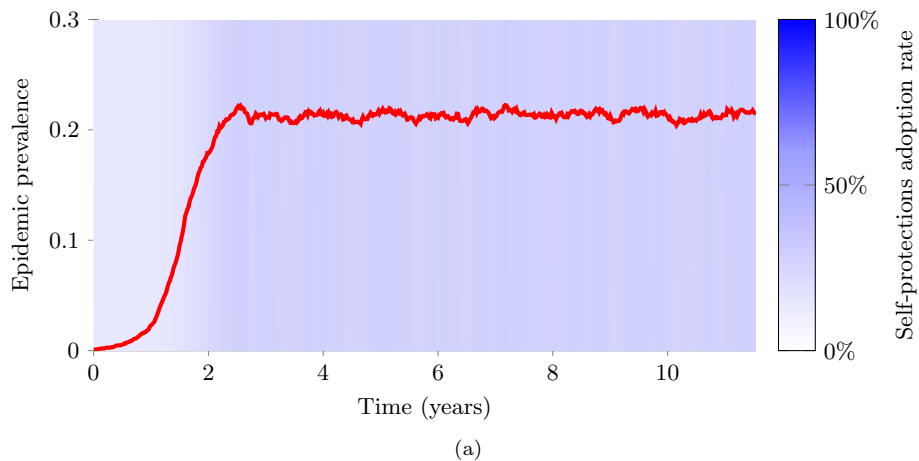


FIG. S6: Simulation of the SIS model in Fig. 2c, in the absence of social influence. In (a) we show the epidemic prevalence  $z(t)$  (red) and fraction of adopters  $\langle x(t) \rangle := \frac{1}{n} \sum_{i \in \mathcal{V}} x_i(t)$  (color intensity of the blue vertical bands); in (b), we show the corresponding trajectories on the phase space. The risk perception function is  $r(z) = 3z^2$ . We observe that, in the absence of social influence, the system converges to an endemic equilibrium with a fraction of population that is adopting self-protections.

- 
- [1] J. Leitch, K. A. Alexander, and S. Sengupta, *Appl. Netw. Sci.* **4**, 105 (2019).
  - [2] N. Perra, B. Gonçalves, R. Pastor-Satorras, and A. Vespignani, *Sci. Rep.* **2** (2012).
  - [3] A. Rizzo, B. Pedalino, and M. Porfiri, *J. Theor. Biol.* **394**, 212 (2016).
  - [4] L. Zino, A. Rizzo, and M. Porfiri, *Phys. Rev. Lett.* **117**, 228302 (2016).
  - [5] E. Valdano, L. Ferreri, C. Poletto, and V. Colizza, *Phys. Rev. X* **5**, 021005 (2015).
  - [6] P. Holme, *Eur. Phys. J. B* **88**, 234 (2015).
  - [7] A. Koher, H. H. K. Lentz, J. P. Gleeson, and P. Hövel, *Phys. Rev. X* **9**, 031017 (2019).
  - [8] P. Van Mieghem, J. Omic, and R. Kooij, *IEEE/ACM Trans. Netw.* **17**, 1 (2009).
  - [9] W. Rugh, *Linear System Theory*, Vol. 2 (Prentice Hall, Upper Saddle River, NJ, 1996).
  - [10] D. J. Watts and S. H. Strogatz, *Nature* **393**, 440 (1998).
  - [11] W. Aiello, F. Chung, and L. Lu, *Exp. Math.* **10**, 53 (2001).
  - [12] J. Mossong, N. Hens, M. Jit, P. Beutels, K. Auranen, R. Mikolajczyk, M. Massari, S. Salmaso, G. S. Tomba, J. Wallinga, *et al.*, *PLOS Med.* **5** (2008).
  - [13] A. Lajmanovich and J. A. Yorke, *Math. Biosci.* **28**, 221 (1976).
  - [14] J. A. Yorke, H. W. Hethcote, and A. Nold, *Sex. Transm. Dis.* **5**, 51 (1978).
  - [15] C. E. Mills, J. M. Robins, and M. Lipsitch, *Nature* **432**, 904 (2004).
  - [16] K. Prem, Y. Liu, T. W. Russell, A. J. Kucharski, R. M. Eggo, N. Davies, S. Flasche, S. Clifford, C. A. B. Pearson, J. D. Munday, *et al.*, *Lancet Public Health* **5**, e261 (2020).
  - [17] M. Nicola, Z. Alsafi, C. Sohrabi, A. Kerwan, A. Al-Jabir, C. Iosifidis, M. Agha, and R. Agha, *Int. J. Surg.* **78**, 185 (2020).
  - [18] J. Qiu, B. Shen, M. Zhao, Z. Wang, B. Xie, and Y. Xu, *Gen. Psychiatr.* **33**, e100213 (2020).
  - [19] A. W. Bartik, M. Bertrand, Z. Cullen, E. L. Glaeser, M. Luca, and C. Stanton, *Proc. Natl. Acad. Sci. USA* **117**, 17656 (2020).
  - [20] H. Markel, H. B. Lipman, J. A. Navarro, A. Sloan, J. R. Michalsen, A. M. Stern, and M. S. Cetron, *JAMA* **298**, 644 (2007).
  - [21] M. C. J. Bootsma and N. M. Ferguson, *Proc. Natl. Acad. Sci. USA* **104**, 7588 (2007).
  - [22] P. Geldsetzer, *Ann. Intern. Med.* **173**, 157 (2020).